Science of the Total Environment 695 (2019) 133805

Contents lists available at ScienceDirect

Science of the Total Environment

journal homepage: www.elsevier.com/locate/scitotenv

Exploiting OMI NO_2 satellite observations to infer fossil-fuel CO_2 emissions from U.S. megacities☆

Daniel L. Goldberg [a,b,*], Zifeng Lu [a,b], Tomohiro Oda [c,d], Lok N. Lamsal [c,e], Fei Liu [c,e], Debora Griffin [f], Chris A. McLinden [f], Nickolay A. Krotkov [e], Bryan N. Duncan [e], David G. Streets [a,b]

[a] Energy Systems Division, Argonne National Laboratory, Lemont, IL, USA
[b] Consortium for Advanced Science and Engineering, University of Chicago, Chicago, IL, USA
[c] Goddard Earth Sciences Technology and Research (GESTAR), University Space Research Association, Columbia, MD, USA
[d] Global Modeling and Assimilation Office, NASA Goddard Space Flight Center, Greenbelt, MD, USA
[e] Atmospheric Chemistry and Dynamics Laboratory, NASA Goddard Space Flight Center, Greenbelt, MD, USA
[f] Air Quality Research Division, Environment and Climate Change Canada, Toronto, Ontario, Canada

HIGHLIGHTS

- Top-down NO_X emissions and inventory-based NO_X-to-CO_2 ratios are used to infer CO_2.
- NO_X and CO_2 emissions are both decreasing, but NO_x is decreasing faster over time.
- Our inferred CO_2 emissions agree well with other top-down methods in the LA basin.

GRAPHICAL ABSTRACT

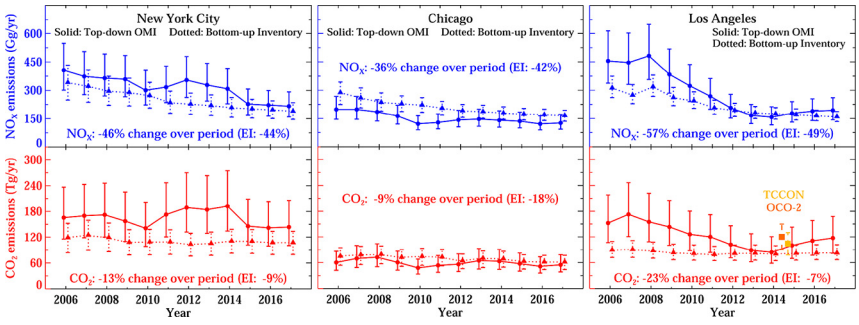

ARTICLE INFO

Article history:
Received 14 May 2019
Received in revised form 15 July 2019
Accepted 5 August 2019
Available online xxxx

Editor: Pavlos Kassomenos

Keywords:
OMI NO_2
NO_x emissions
CO_2 emissions
Top-down emissions

ABSTRACT

Fossil-fuel CO_2 emissions and their trends in eight U.S. megacities during 2006–2017 are inferred by combining satellite-derived NO_X emissions with bottom-up city-specific NO_X-to-CO_2 emission ratios. A statistical model is fit to a collection NO_2 plumes observed from the Ozone Monitoring Instrument (OMI), and is used to calculate top-down NO_X emissions. Decreases in OMI-derived NO_X emissions are observed across the eight cities from 2006 to 2017 (−17% in Miami to −58% in Los Angeles), and are generally consistent with long-term trends of bottom-up inventories (−25% in Miami to −49% in Los Angeles), but there are some interannual discrepancies. City-specific NO_X-to-CO_2 emission ratios, used to calculate inferred CO_2, are estimated through annual bottom-up inventories of NO_X and CO_2 emissions disaggregated to 1×1 km^2 resolution. Over the study period, NO_X-to-CO_2 emission ratios have decreased by ~40% nationwide (−24% to −51% for our studied cities), which is attributed to a faster reduction in NO_X when compared to CO_2 due to policy regulations and fuel type shifts. Combining top-down NO_X emissions and bottom-up NO_X-to-CO_2 emission ratios, annual fossil-fuel CO_2 emissions are derived. Inferred OMI-based top-down CO_2 emissions trends vary between +7% in Dallas to −31% in Phoenix. For 2017, we report annual fossil-fuel CO_2 emissions to be: Los Angeles 113 ± 49 Tg/yr; New York City 144 ± 62 Tg/yr; and Chicago

☆ The submitted manuscript has been created by UChicago Argonne, LLC, Operator of Argonne National Laboratory ("Argonne"). Argonne, a U.S. Department of Energy Office of Science laboratory, is operated under Contract No. DE-AC02-06CH11357. The U.S. Government retains for itself, and others acting on its behalf, a paid-up nonexclusive, irrevocable worldwide license in said article to reproduce, prepare derivative works, distribute copies to the public, and perform publicly and display publicly, by or on behalf of the Government.

* Corresponding author at: Milken Institute School of Public Health, George Washington University, Washington, DC, USA.
E-mail address: dgoldberg@gwu.edu (D.L. Goldberg).

https://doi.org/10.1016/j.scitotenv.2019.133805

55 ± 24 Tg/yr. A study in the Los Angeles area, using independent methods, reported a 2013–2016 average CO_2 emissions rate of 104 Tg/yr and 120 Tg/yr, which suggests that the CO_2 emissions from our method are in good agreement with other studies' top-down estimates. We anticipate future remote sensing instruments – with better spatial and temporal resolution – will better constrain the NO_X-to-CO_2 ratio and reduce the uncertainty in our method.

1. Introduction

Carbon dioxide (CO_2) emissions from fossil fuel combustion are the main cause for the observed increase in atmospheric CO_2 concentration and subsequent global warming (Hansen et al., 1981; IPCC, 2013). Due to CO_2's central role in global warming, it is critical to understand the quantities of anthropogenic fossil-fuel CO_2, so that policymakers can better devise strategies to reduce its emissions and warming effect on the globe.

Urban areas account for approximately 70% of fossil-fuel CO_2 emissions globally (International Energy Agency, 2008). Despite the large role of urban CO_2 emissions in the total global carbon budget, there are gaps in our current understanding of urban dynamics that cause their emissions (Mitchell et al., 2018). Fossil-fuel CO_2 emissions are often reported at national or regional scales rather than locally because energy usage data are often provided at aggregated spatial scales, and are reported with widely varying guidelines and procedures. Downscaled CO_2 emissions have been developed globally by applying spatial surrogates to national or regional emissions inventories, and are considered an important first step in estimating the spatial allocation of CO_2 emissions (Gately et al., 2015; Gurney et al., 2012; Nangini et al., 2019; Oda et al., 2018; Oda and Maksyutov, 2011; Patarasuk et al., 2016). The uncertainties associated with downscaled emissions in urban areas could be substantial (>20%) (Gately and Hutyra, 2017; Gurney et al., 2019).

To better refine the magnitude and spatial heterogeneities of the fossil-fuel CO_2 emissions from urban areas, intensive experimental field campaigns have been conducted over megacities. These techniques are loosely defined as a "top-down" approach of constraining emissions. These campaigns use aircraft and other in situ observations to calculate a CO_2 flux from the metropolitan area (Lauvaux et al., 2016; Mitchell et al., 2018; Sargent et al., 2018; Turnbull et al., 2018).

While experimental field campaigns often generate accurate CO_2 flux estimates, a disadvantage of intensive field campaigns is that they often: involve many active measurements, focus on short time periods, are located over a single area, and need to be combined with model simulation output at high spatiotemporal resolution in order to calculate emission fluxes. Instead, satellite data can be more useful to derive "top-down" long-term trends over larger spatial extents. Japan's Aerospace Exploration Agency's (JAXA) Greenhouse gases Observing SATellite (GOSAT) and NASA's Observing Carbon Observatory 2 (OCO-2) are two current satellite instruments, which have long-term measurements (4+ years) of column-averaged CO_2 mixing ratios (XCO_2) over cloud and aerosol free scenes (Crisp et al., 2004; Kuze et al., 2009). Studies have used these two satellite instruments to: derive regional fluxes of CO_2 (A. Eldering et al., 2017; Hakkarainen et al., 2016; Hammerling et al., 2012), estimate annual CO_2 emissions from individual megacities (Kort et al., 2012; Schwandner et al., 2017), derive emissions from power plants (Nassar et al., 2017), and estimate CO_2 emissions from wildfires (Guo et al., 2017; Konovalov et al., 2014). However, the swaths of OCO-2 and GOSAT are much narrower than other polar-orbiting satellite instruments routinely used to monitor tropospheric trace gas column amounts, such as OMI (Levelt et al., 2006). As a result, it is difficult to get multiple overlapping swaths over many locations on the globe using OCO-2 or GOSAT in isolation.

Instead, one can use satellite instruments with greater spatial coverage in lieu of a satellite that directly measures CO_2 and apply conversion factors to calculate CO_2 from co-emitted species, such as NO_X and CO (Berezin et al., 2013; Konovalov et al., 2016). Ideally, one would use emissions ratios derived from satellite data to convert NO_X emissions, but since current CO_2-observing satellites have narrow swaths, there are limited instances of this (Reuter et al., 2019); instead, we must instead rely on bottom-up emissions ratios. Using a combination of OMI NO_2 and bottom-up NO_X-to-CO_2 emissions ratios, Berezin et al. (2013) found an underestimate of the CO_2 bottom-up emissions in China, while Konovalov et al. (2016) found a slight overestimate of CO_2 bottom-up emissions in western Europe.

Using NO_2 to calculate CO_2 emissions can be especially powerful because NO_2 has a short lifetime and is better representative of local anthropogenic emissions than an atmospheric trace gas with a longer lifetime, such as CO. Furthermore, using NO_2 to calculate CO_2 emissions allows us to quantify fossil-fuel CO_2 emissions in the presence of biogenic CO_2, which is often a challenge in other CO_2 top-down studies (Ye et al., 2017).

In this study, we take advantage of the relatively short lifetime of NO_X during the warm season (April–September) and the fact that NO_X is co-emitted with CO_2 during fossil-fuel combustion, to indirectly calculate fossil-fuel based CO_2 emissions for eight megacities in the United States. We do this by first calculating the annual NO_X emissions for each of these cities using an approach outlined and refined in previous literature (Goldberg et al., 2019; Lu et al., 2015), as discussed in the Methods and data section. We then apply city-specific CO_2-to-NO_X conversion factors, which are generated from the EPA state-level bottom-up emissions. While there are uncertainties associated with the both the top-down NO_X emissions and the CO_2-to-NO_X conversion factors, we carefully account for these during our calculation, as discussed in the Methods and data section. Furthermore, an advantage of this technique over others (Berezin et al., 2013; Konovalov et al., 2016) is that we do not rely on a chemical transport model, which eliminates the forecasted winds and chemical mechanism of the model as sources of uncertainty.

2. Methods and data

2.1. OMI NO_2

For this project, we use remotely sensed NO_2 measurements from OMI. OMI is a Dutch-Finnish UV–Vis spectrometer on the polar-orbiting NASA Aura satellite (Levelt et al., 2006, 2018). OMI NO_2 slant column densities are derived from backscattered radiance measurements in the 405–465 nm spectral window of the UV–Vis spectrometer. OMI measures backscatter radiances in a 2600 km swath with a nadir (center of the swath) pixel size of 13×24 km^2. The instrument acquires once-daily snapshots in the mid-afternoon (~13:45 local time) at each location on the globe. Since the development of the "row anomaly" in 2007 (Dobber et al., 2008), which obstructs ~30% of the field of view, it now has global coverage once every 2–3 days.

OMI NO_2 satellite data version 3.1 is operationally released by NASA (Krotkov et al., 2017). We filter the Level 2 OMI NO_2 data to ensure only valid pixels are used. Daily pixels with solar zenith angles ≥80°, cloud radiance fractions ≥0.5, or surface albedo ≥0.3 are removed as well as the five largest pixels at the swath edges (i.e., pixel numbers 1–5 and 56–60). We also remove any pixel flagged by NASA including pixels with NaN values and those affected by the row anomaly. We further

re-process the operational slant column density data to create tropospheric vertical column density data using high spatial resolution air mass factors (AMFs) as provided by Environment Canada (McLinden et al., 2014). AMFs are quantities used to convert the slant column data directly observed by the satellite instrument to vertical column data, which is more representative of surface concentrations and emissions. The AMFs are a function of NO_2 vertical column profiles as provided by a chemical transport model and scattering weights from a radiative transfer model (which are a function of satellite viewing angle, surface albedo, aerosols, and clouds). For the re-processed AMFs in this study, we use a 10×10 km^2 Global Environmental Multi-scale – Modelling Air quality and CHemistry (GEM-MACH) model simulation (Akingunola et al., 2018) to provide NO_2 profile shapes below 2 km in altitude, and above 2 km, NO_2 profile shapes from a global chemical transport model (GEOS-Chem) are used since they include lightning NO_X emissions. The emissions used to drive the GEM-MACH simulation are representative of 2006; see McLinden et al. (2014) for details. Tropospheric vertical column data are 25–100% larger in magnitude and more accurate in urban areas when using a regional model to re-process the AMFs (Goldberg et al., 2017; Laughner et al., 2019). The uncertainty in any daily measurement in the operational v3.1 data has been assigned to be approximately 1.0×10^{15} molecules-cm^{-2} (Krotkov et al., 2017). This equates to roughly a 10–20% uncertainty over polluted areas. However, because we are oversampling over many days (>200 days), we assume that random errors will cancel due to the large number of observations used. This leaves only the systematic errors. Here, we assign the AMFs and tropospheric vertical column contents a systematic uncertainty of 20% following McLinden et al. (2014).

2.2. NO_X emissions calculation

We use a top-down inverse statistical modeling technique to directly derive NO_X emissions from a combination of satellite data and re-analysis meteorology. In this method, all NO_2 satellite data over individual city centers or "hotspots" are compiled and rotated based on the daily-observed wind direction, so that the oversampled plume is decaying in a single direction. For our calculation, we only utilize days in which there is a valid NO_2 retrieval (cloud radiance fraction <0.3 and not affected by the row anomaly) and in which average wind speeds in the lowest 8 model layers of the ERA-Interim re-analysis (approximately 0–500 m above the surface) (Dee et al., 2011) are >3 m/s. For cities in the northeastern US – New York City and Washington, DC – we only utilize data when the wind directions are from the NW or SE to minimize influence from nearby cities, which are SW/NE of each other. We then integrate NO_2 vertical column data perpendicularly across the plume to calculate line densities; across plume widths (integration limits) vary by metropolitan area – for New York City and Los Angeles, they are 200 km, for Chicago it is 150 km, and 100 km for all other cities. The line densities, which are parallel to the wind direction, peak near the primary NO_X emissions source and gradually decay downwind as the NO_X is transformed into different chemical species or deposited to the surface. The line densities are fit to a statistical exponentially modified Gaussian (EMG) model (Beirle et al., 2011; de Foy et al., 2014; Valin et al., 2013). The parameters from the fit are then used to calculate the NO_2 burden and effective photochemical lifetime. Finally, the NO_X emissions rate from the primary source can be calculated from the two aforementioned fitted parameters and the NO_X/NO_2 ratio, which is assumed to be 1.33 (Beirle et al., 2011; Valin et al., 2011).

This method can only be applied when NO_2 is photochemically active and the NO_2 lifetime is short. Therefore, we only use OMI NO_2 data from April–September. We do not expect any significant systematic biases from only using April–September data. Reported emissions data shows that power generation in the U.S. (and thus pollutant emissions from the power sector) peaks in July and is lowest in April. This may yield a positive +10% bias in the top-down NOx emissions attributed to the power sector, however, the power sector often represents <20% in cities (see Fig. 2). For all other sectors (transportation, manufacturing, etc.), we assume no seasonality in emissions.

The error associated with this top-down fit is calculated to be 35%, and is a combination of the errors associated with the satellite data itself (20%), the statistical uncertainty from the EMG fit (10%), sensitivity to various parameters such as lifetime and across plume width (20%), the wind speed and direction (10%), and the NO_x/NO_2 ratio (15%). For the trend analysis, this uncertainty is much reduced, since the systematic uncertainties in the emissions do not have to be considered, thus leaving only the random EMG fitting error of roughly 10%. For further information on this method or the uncertainties associated with this method, please see other literature (de Foy et al., 2014; McLinden et al., 2014; Goldberg et al., 2019; Lu et al., 2015).

2.3. Bottom-up emissions estimates

To calculate our CO_2-to-NO_X emissions ratios, we use "bottom-up" emissions inventories for 2005–2017 as provided by the U.S. EPA. We account for regional differences in emissions by using bottom-up data developed at the state and sector levels. The state-level data accounts for the varying industries in the state and the varying types and ages of vehicles registered. It is important to use emissions data compiled at the state level because there can be large regional differences in regulations, economic activity, and lifestyle that can cause substantial variation in per capita emissions (Gately et al., 2015; Gurney et al., 2019).

For NO_X, we take the state-by-state and sector-by-sector emissions as provided by the Air Pollutant Emissions Trends Data (https://www.epa.gov/air-emissions-inventories/air-pollutant-emissions-trends-data). Data for 2005, 2008, 2011 and 2014 are provided by the most up-to-date versions of EPA's National Emissions Inventory (NEI); for non-power plant sectors, the years in between are interpolated by EPA. Using the annual state-level emissions data, we spatially allocate the emissions to a 1×1 km^2 horizontal resolution using the following procedure: for power plant emissions we use annual continuous emission monitoring system (CEMS) data (https://ampd.epa.gov/ampd/) and match each power plant to the closest 1×1 km^2 grid point; for on-road mobile sources emissions, we spatially allocate based on a 1×1 km^2 road density network; for all other sources including industrial fuel combustion, off-road vehicles, and residential heating, we spatially allocate the emissions based on each state's 1×1 km^2 gridded population. We do not include wildfire or biogenic sources of NO_X in our bottom-up emissions as these sectors are minimal contributors in major city centers – the focus of our work.

For CO_2, we acquire the data from EPA's State CO_2 Emissions from Fossil Fuel Combustion (https://www.epa.gov/statelocalenergy/state-co2-emissions-fossil-fuel-combustion), which are based on energy consumption data from EIA's State Energy Data System and is reported annually and on a similar state-by-state and sector-by-sector basis. Data is spatially allocated using the same procedure for NO_X outlined above. To maintain consistency with the NO_X bottom-up emissions, no wildfire or biogenic sources are included in our spatially allocated CO_2 bottom-up emissions. CO_2 bottom-up emissions data is only available through 2016, so for 2017 we assume bottom-up CO_2 emissions to be identical to 2016 emissions.

2.4. Top-down CO_2 emissions calculation

The OMI top-down NO_X emissions are divided by the city-specific NO_X-to-CO_2 bottom-up emissions ratio to get fossil-fuel based CO_2 emissions. To develop the city-specific NO_X-to-CO_2 emissions ratios, we aggregate the 1×1 km^2 bottom-up emissions to a city-specific radius (varies between 50 and 75 km; 75 km for New York City and Los Angeles, 62.5 km for Chicago, and 50 km for all other cities) around the city center to minimize any artificial spatial heterogeneities. After aggregating the bottom-up emissions, we compute the ratio. We estimate the error associated with this ratio to be 25%. The total error associated with the top-down CO_2 emissions fit is 43% and is computed by

taking the square root of the sum of errors associated with the top-down NO_X fit and NO_X-to-CO_2 ratio.

3. Results and discussion

3.1. NO_X and CO_2 bottom-up emissions inventories

Fig. 1 shows the annual bottom-up NO_X and CO_2 emissions disaggregated to 1×1 km^2 and the difference between 2005 and 2016 emissions. Dominant sources of NO_X and CO_2 are clearly visible in urban areas and along major transportation routes. While perhaps less identifiable, emissions from power plants are also included. There are clear downward trends in NO_X emissions in almost all areas during this 12-year period, likely due to a combination of more effective NO_X-conversion technologies (e.g., selective catalytic reduction, catalytic converters), as well as switches to more NO_X-efficient combustion techniques (e.g., low-NO_X boilers, switches to fossil fuels that emit less NO_X per unit of energy) (de Gouw et al., 2014). For CO_2 emissions, the trends are mixed: in east coast, northern Midwest, and west coast states (e.g., New York, Illinois, California), the reported CO_2 emissions have dropped, while in many central US states (e.g., Texas, North Dakota, Colorado) the reported CO_2 emissions have increased. This may be related to the increase in oil & gas activities in these areas over this period. In states where there are increases in CO_2 emissions, but decreases in NO_X emissions (e.g., Texas), it appears that NO_X-control strategies more than compensated for the reported increase in fossil-fuel usage.

We also separate the spatially disaggregated bottom-up inventory into three different sectors: power plants in the CEMS database, on-road mobile sources, and all other sources (e.g., industrial fuel combustion, off-road vehicles, and residential heating). Each sector's individual contribution to the total emissions can vary substantially by grid box. For that reason, we calculate each sector's contribution to the total emissions within each grid box. These are then aggregated to 100×100 km^2 grid boxes and shown in Fig. 2. In most rural areas, emissions from transportation dominate – especially in areas with no power plants or agricultural activities. In urban areas, the mix is more even. For example, in New York City, non-on-road transportation and non-power plant emissions represent the largest fraction of emissions (~40%), while on-road transportation (~35%) and power plant (~25%) emissions are also non-trivial. This is important information for our uncertainty analysis because the spatial disaggregation of NO_X and CO_2 emissions are known with the most certainty from power plants, with medium-certainty from vehicles, and with low certainty from all other sources.

3.2. NO_X-to-CO_2 emissions ratios

Fig. 3 shows the annual NO_X-to-CO_2 ratios across the US for 2005 and 2016 as well as the interannual trends of the ratio for eight cities spread

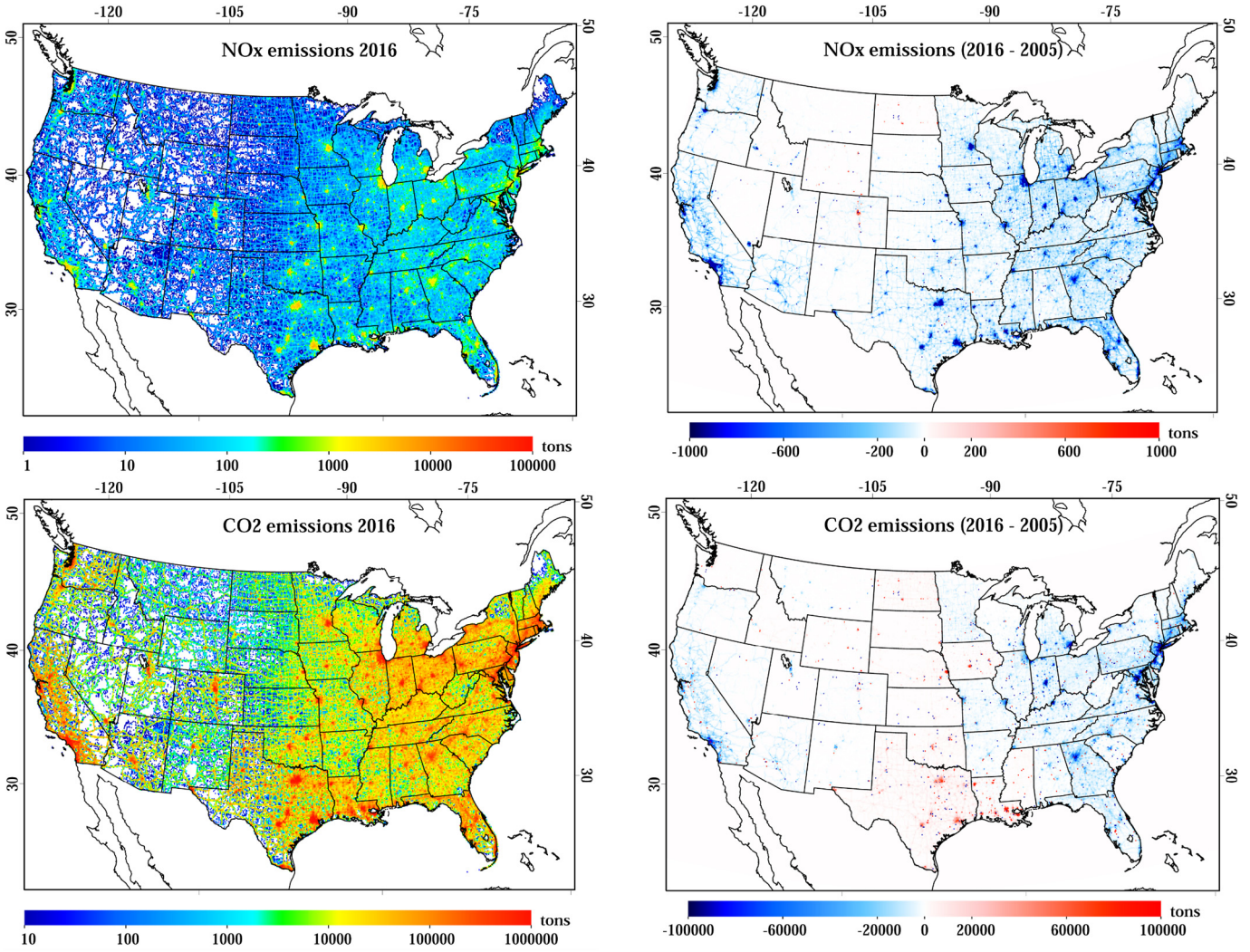

Fig. 1. Bottom-up emissions for (top) NO_X and (bottom) CO_2 spatially allocated to 1×1 km^2. (Left) Annual emissions for 2016. (Right) Difference between annual emissions between 2016 and 2005.

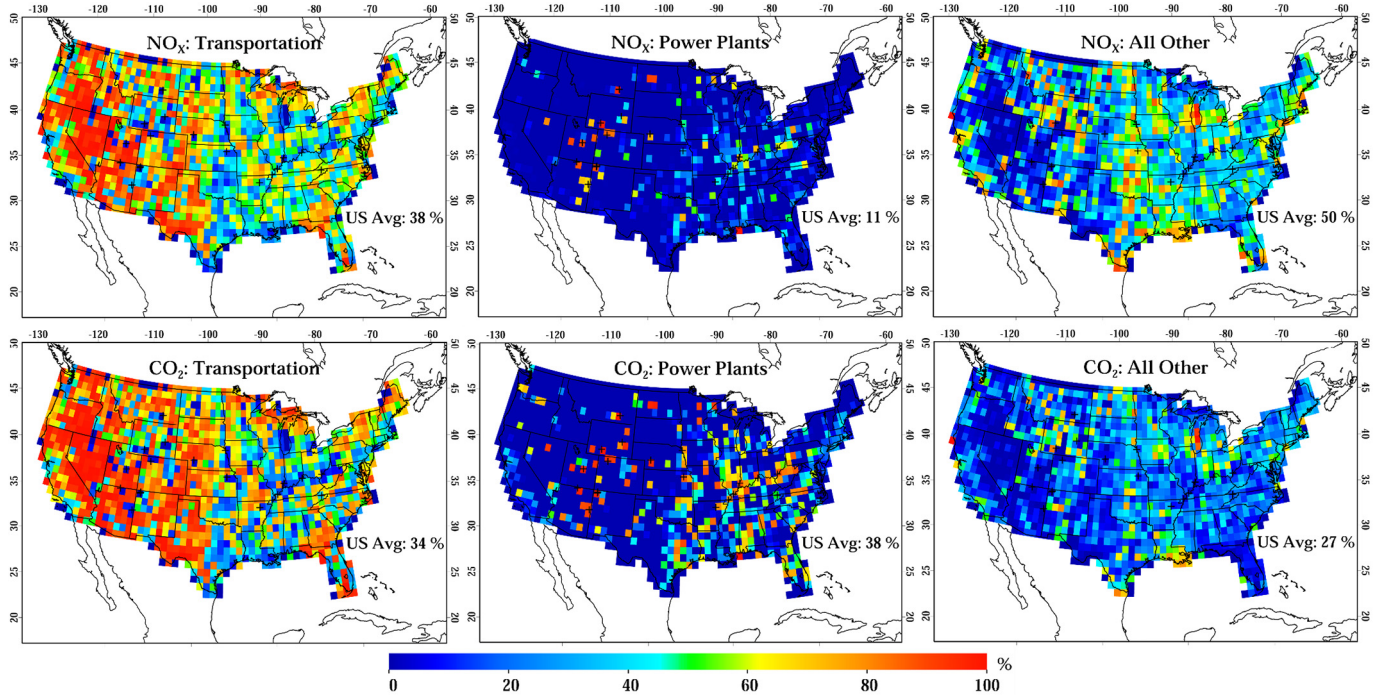

Fig. 2. Each sector's individual contribution to the total emissions by percentage for 2016 aggregated to 100 × 100 km^2 for (top) NO_X emissions and (bottom) CO_2 emissions. Left panels represent the transportation sector, center panels represent power plants in the CEMS, and right panels represent all other sources.

across the United States between 2005 and 2016. The spatial figures show the ratio aggregated to 100 × 100 km^2, while the city-specific ratios represent the area within a 50–75 km radius of the city center depending on the size of the city (75 km for New York City and Los Angeles, 62.5 km for Chicago, and 50 km for all other cities). In the spatial plots, the NO_X-to-CO_2 ratios have decreased over time as NO_X emissions are reduced nationwide (Fig. 1) due to NO_X-control technologies and economic shifts of fuel types, while CO_2 emissions have decreased only modestly primarily due to economic-based shifts away from coal combustion and increases in vehicle combustion efficiency. Areas with no CO_2 or NO_X emissions in >90% of the 100 × 100 km^2 box are removed. The NO_X-to-CO_2 ratios are lowest near large and isolated power plants denoted on the spatial plots because large power plants typically remove >95% of their NO_X emissions using advanced control technologies (e.g., selective catalytic reduction). The NO_X-to-CO_2 ratios are also relatively low in the largest metropolitan areas (e.g., New York City, Los Angeles, Chicago), which have more actively reduced their NO_X emissions due to their metropolitan areas' legacy of exceedances of the surface O_3 standard. The NO_X-to-CO_2 ratios are highest in the Central Plains' and northern Rockies' states; this is due to a lack of monitoring of NO_X from transportation in these states (Fig. 4) and less stringent NO_X regulations due to their current attainment of the surface O_3 standards.

According to the bottom-up emissions, the NO_X-to-CO_2 ratio has decreased by approximately 40% nationwide over the 12-year period, although there are some states, which have reduced their NO_X-to-CO_2 ratio >50% (i.e., Texas, California, and New York), while other states have seen small decreases or slight increases (i.e., Colorado, Wyoming, and North Dakota) potentially due to industrial activities related to natural gas fracking. Of the eight cities we focus on, New York City has the

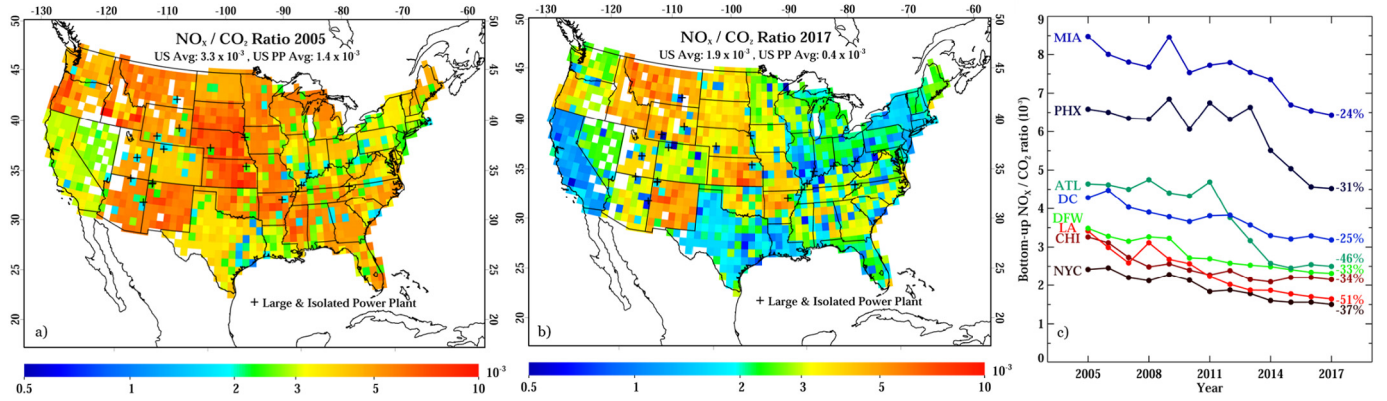

Fig. 3. The annual NO_X-to-CO_2 emissions ratio based on the EPA NEI for NO_X and the EPA state bottom-up emissions for CO_2 for (a) 2005 and (b) 2017. The spatial bottom-up emissions are aggregated to 1° × 1° grid boxes, and then the ratio is computed. Areas outside of the continental United States and areas with no emissions in >90% of the 1° × 1° box are removed. (c) The annual NO_X-to-CO_2 emissions ratio between 2005 and 2017 for eight metropolitan areas in the United States are shown. Ratios are representative of a 50–75 km radius around the city center.

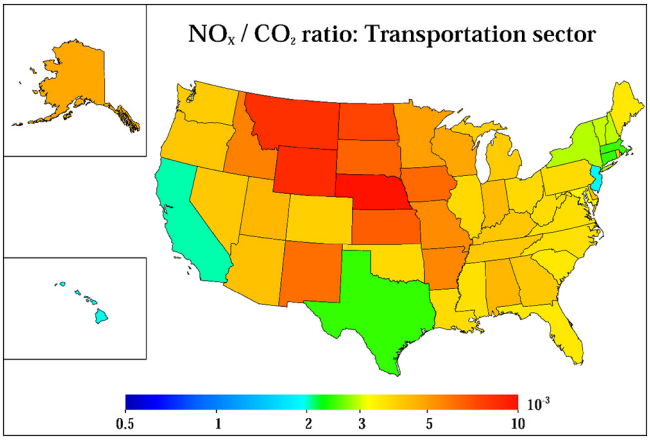

Fig. 4. State reported NO_X/CO_2 ratios for the transportation sector in 2015.

lowest reported NO_X-to-CO_2 ratio throughout the majority of the 2005–2016 period, while Los Angeles has the largest decrease in the ratio during the same thirteen-year timeframe (Fig. 3).

3.3. OMI NO_X emissions estimates for major US cities

Top-down OMI NO_X estimates have been generated for eight major cities in the United States; these estimates are shown in Table 1 (all years are shown in Table S1). The OMI NO_X estimates are 3-year averages during the warm season (April–September) centered on the year of interest (approximately 150–300 valid retrievals per 549-day period depending on the year and location). Bottom-up emissions that are temporally allocated suggest that emissions between 12 and 3 PM – the time of the OMI overpass – are 30–50% larger than the 24-hour average reported by the annual bottom-up emissions (Goldberg et al., 2019). For that reason, we divide the top-down emissions by a factor of 1.4 for these US cities in order to conduct a fair comparison with the annual bottom-up emissions. For the bottom-up emissions, we gather the total emissions within a specified radius of the city center – 75 km for New York City and Los Angeles, 62.5 km for Chicago, and 50 km for all other cities. These radii were estimated based on plume width in the top-down approach.

For the rest of this paper, we focus on the three largest metropolitan areas in the United States – New York City, Los Angeles, and Chicago – as these areas have the most robust results due to the large magnitude of their NO_2 plumes, which are easily differentiated from diffuse background sources. Fig. 5 depicts the rotated OMI NO_2 plume and subsequent top-down NO_X derivation from these three cities for the 3-year average centered on 2006. Heterogeneous topography and regional mountain/sea/lake breezes are effects that may shorten the effective photochemical lifetime and bias the top-down emissions calculation. We partially account for this bias by only selecting days with strong winds (>3 m/s); on days with faster winds speeds, the mountain/sea/lake breezes are secondary to the synoptic flow. Our top-down NO_X emissions may be too large in later years since we are using AMFs derived from a chemical transport model simulation driven by 2006 emissions; we expect this bias to be about +10% in later years. Future work will be focused on deriving long-terms trends of NO_X using model simulations driven by year-varying emissions (Laughner et al., 2019; Silvern et al., 2019).

Fig. 6 depicts the NO_X estimates for our three focus cities from 2006 through 2017. For Los Angeles, our top-down approach suggests a decline in NO_X emissions by 57% between 2006 and 2017, while the bottom-up emissions suggest a decline of 48% over the same period. Our results suggest an underestimate in the NO_X bottom-up emissions during the early period and better agreement in the more recent years. For New York City and Chicago, both the top-down estimates have similar trends – a sharp decline in NO_X emissions between 2006 and 2010, and a leveling off since then. The NO_X bottom-up emissions do not capture this bifurcated trend. These results are consistent with recent literature suggesting that NO_X emissions across much of the United States declined quicker than anticipated between 2008 and 2010 due to the economic recession (de Foy et al., 2016; Russell et al., 2012; Tong et al., 2016) and then slower than expected since 2011 (Jiang et al., 2018). However, the trends during the entire 12-year period match the bottom-up trends well for both cities.

3.4. "OMI" CO_2 emissions estimates for major US cities

We then calculate the top-down "OMI" CO_2 emissions for these major metropolitan areas using the top-down OMI NO_X estimates and the NO_X-to-CO_2 ratios suggested by the bottom-up emissions. The bottom panels of Fig. 6 illustrate these values and trends. For New York City, CO_2 emissions decreased from 165 ± 71 Tg/yr in 2006 to 144 ± 62 Tg/yr in 2017 and represent a 13% decrease over the 12-year period. For Chicago, CO_2 emissions decreased modestly from 60 ± 26 Tg/yr in 2006 to 55 ± 24 Tg/yr in 2017 and represent a 9% decrease over the 12-year period. The magnitude of the change in New York City and Chicago over the 12-year period is similar to the bottom-up emissions; however, this 12-year trend is not indicative of the interannual trends in both cities. Between 2006 and 2008 there is a slight increase, a sharp decrease in 2009 and 2010 due to the economic downturn, a temporary increase between 2010 and 2014 due to the economic recovery and a stabilization since then. For Los Angeles, CO_2 emissions are 147 ± 63 Tg/yr in 2006 and decrease to 81 ± 35 Tg/yr by 2014, and then increase slightly to 113 ± 49 Tg/yr in 2017, representing a 23% decrease over this 12-year period, while the bottom-up emissions suggest a 7% decrease over the same time frame.

For Los Angeles, we can compare our result to other top-down studies – satellite and in situ. For a 2013–2016 average, Hedelius et al. (2018) suggest a top-down estimate of 104 ± 26 Tg/yr using in situ monitors from the Total Carbon Column Observing Network and 120 ± 30 using OCO-2 July 2013–August 2016. We report a value of 96 ± 41 Tg/yr in 2015. Values reported by Hedelius et al. (2018) are larger than the mean values reported here; however, our estimates representative of a smaller spatial domain. The aforementioned studies quantify CO_2 emissions over a larger area that include portions of the California Central Valley and the San Diego metropolitan area, while our study quantifies CO_2 from only the Los Angeles basin. Second, our study only quantifies CO_2 emissions from fossil-fuel combustion, and not the total

Table 1
Top-down OMI NO_X and OMI CO_2 emissions for 2006 and 2017 compared to the bottom-up NO_X and CO_2 emissions for the eight metropolitan areas of interest. Data for all years can be found in Table S1.

City	Inventory	NO_x (Gg/yr)			CO_2 (Tg/yr)		
		2006	2017	% change	2006	2017	% change
New York City	Top-down	407	216	−46.9%	165	144	−13.1%
	Bottom-up	340	188	−44.6%	119	107	−9.5%
Chicago	Top-down	197	126	−35.8%	60	55	−9.0%
	Bottom-up	287	165	−42.5%	75	61	−18.2%
Los Angeles	Top-down	445	193	−56.7%	147	113	−23.0%
	Bottom-up	261	134	−48.6%	72	67	−6.6%
Dallas	Top-down	64	48	−25.2%	20	21	6.5%
	Bottom-up	128	96	−24.9%	33	35	6.9%
Atlanta	Top-down	61	35	−42.9%	13	13	0.0%
	Bottom-up	77	47	−39.3%	14	15	6.3%
Washington, DC	Top-down	82	43	−47.3%	18	13	−26.3%
	Bottom-up	94	54	−42.7%	18	15	−19.2%
Miami	Top-down	56	46	−16.9%	7	7	4.0%
	Bottom-up	54	41	−24.5%	6	6	−5.5%
Phoenix	Top-down	78	39	−49.6%	14	10	−31.1%
	Bottom-up	53	37	−29.2%	8	8	−3.1%

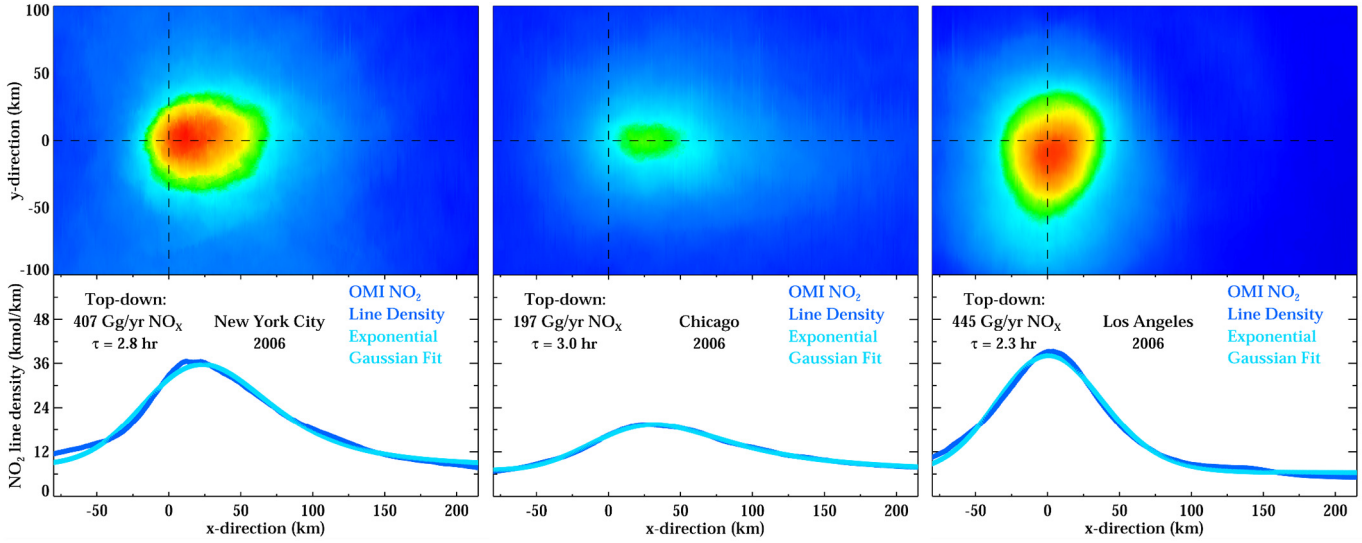

Fig. 5. Top row panels represent the oversampled (1×1 km^2) OMI NO_2 plumes from our three metropolitan areas of focus (New York City, Chicago, and Los Angeles) rotated based on wind direction over a non-continuous 18-month period, Apr–Sept 2005–2007 centered on 2006. Second row panels represent the OMI NO_2 line densities integrated over the across plume width (for NYC & LA: −100 km to 100 km along the y-axis of the top panels, Chicago: −75 km to 75 km) and the corresponding EMG fit for the 18-month period shown in the top panels; NO_X emissions estimates are in units of Gg/yr NO_2 equivalent.

CO_2 emissions. Our method is unable to quantify CO_2 emitted from land-use changes, but we expect these net changes on annual basis to be small in a major metropolitan area. More recently, Cui et al. (2019) calculated a fossil-fuel CO_2 flux of 124 ± 31 Tg/yr between June 2013–May 2014 for the South Coast Basin, but it is unclear how they defined the South Coast basin.

It is also important to note the uncertainty from our method is larger than other studies (i.e., ~43% uncertainty in our study vs. ~25% uncertainty in Hedelius et al. (2018) and Cui et al. (2019)). The cause of our larger uncertainty is due to our reliance on the bottom-up emissions inventory for the NO_X to CO_2 ratio. Unfortunately, emissions from low certainty sources (e.g., industrial activities) are often widespread in major urban areas and generally have larger NO_X-to-CO_2 ratios than sources with known emissions such as power plants (Fig. 7). While bottom-up ratios may be not identically representative of reality, we do account for regional variations of the NO_X-to-CO_2 ratio, which have large spatial heterogeneities and are due to widely varying regulations, economic activities, and lifestyles. In the future, the simultaneous use of satellite NO_2 and CO_2 measurements to derive the ratio will be preferable, but currently there are only a few collocated enhancements over cities and there are other uncertainties inherent in using collocated satellite data to derive the ratio (Reuter et al., 2019). With that said, it is encouraging that we show good agreement with other top-down studies in Los Angeles; therefore, we believe that our initial estimates of the uncertainty may be conservative.

4. Conclusions

In this study, we calculate fossil-fuel CO_2 emissions and their trends in eight U.S. megacities during 2006–2017 by combining satellite-derived NO_X emissions with bottom-up city-specific NO_X-to-CO_2 emission ratios. Decreases in OMI-derived NO_X emissions are observed across studied cities from 2006 to 2017 (−17% in Miami to −58% in Los Angeles), and are consistent with bottom-up inventories (−25% in Miami to −49% in Los Angeles). Combining top-down NO_X emissions and bottom-up NO_X-to-CO_2 emission ratios, annual fossil-fuel CO_2 emissions are derived. OMI-based top-down CO_2 emissions trends vary between +7% in Dallas to −31% in Phoenix. Good agreement of CO_2

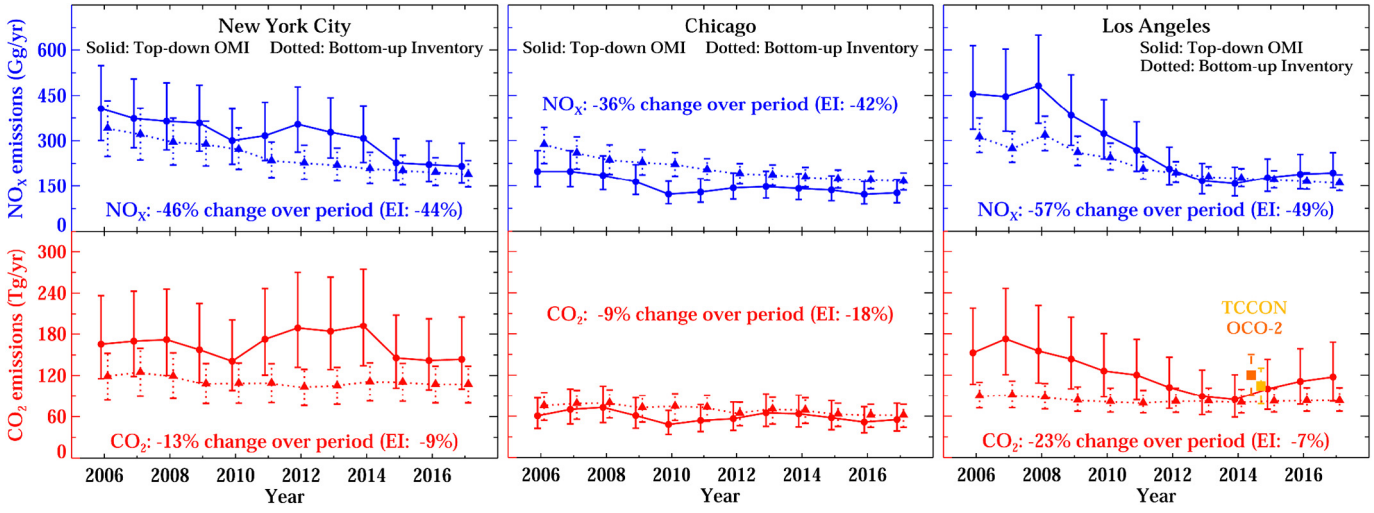

Fig. 6. Third row panels depict top-down OMI NO_X trends (solid line), and bottom-up emissions (dotted line) between 2006 and 2017. Bottom row panels depict trends of top-down "OMI" CO_2 trends (solid line) and bottom-up emissions (dotted line) during the same timeframe. A description of the uncertainty calculations can be found in the Methods and Data section.

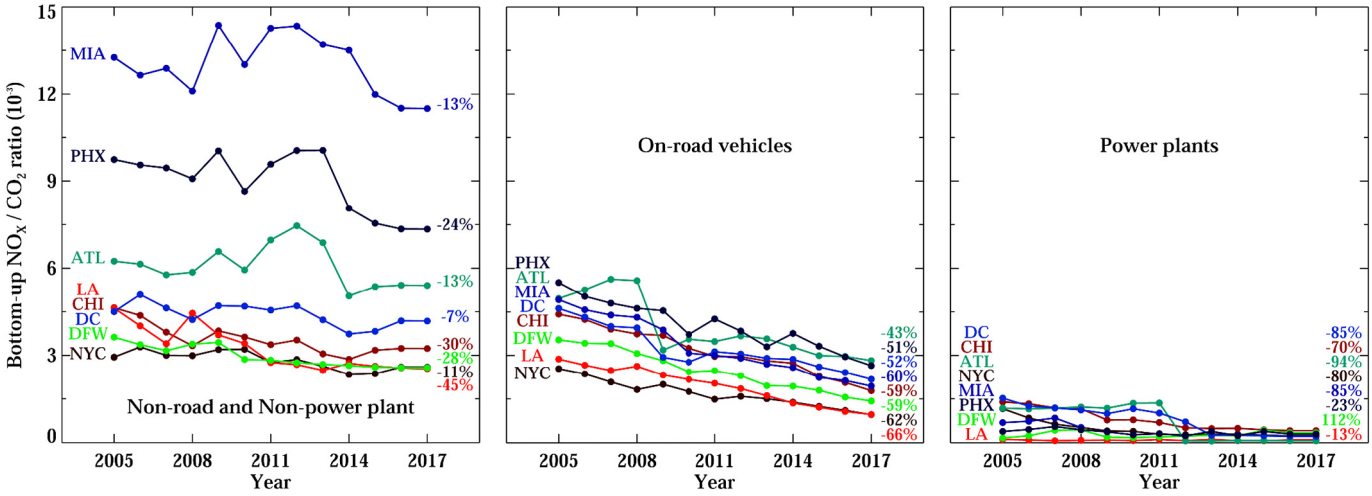

Fig. 7. Reported annual bottom-up NO_X-to-CO_2 ratios by sector for the eight metropolitan areas of interest.

emissions is found in comparison with other studies' top-down estimates in Los Angeles.

The distinct advantage of our methodology is the ability to apply it to any large metropolitan area extending back to 2005 (and potentially earlier if using other satellite datasets such as SCIAMACHY) with no new additional measurements needed. In this manner, we can calculate top-down trends in CO_2 with some certainty. In particular, we note an increase in CO_2 emissions in New York City and Chicago between 2009 and 2014 that is not captured in the bottom-up emissions inventory. This increase is in alignment with the economic recovery following the U.S. recession in 2008.

Our method works best for cities with consistently large NO_2 plumes, isolation from other large cities, homogenous topography, and reasonable bottom-up NO_X and CO_2 emissions. Although we focus on metropolitan areas in the United States, this technique can be applied to other metropolitan areas across the globe. If investigating a region with bottom-up emissions that are more uncertain, the top-down CO_2 estimates will also be more uncertain.

Future applications of this technique may be of most interest to policymakers of cities who want to better quantify changes in their carbon footprint over decadal timeframes, and track progress towards climate goals. Satellite data, as a stand-alone product, should not be used determine compliance, but instead could be used as one of many metrics to assess progress. New remote sensing instruments with higher spatial resolution and higher signal-to-noise ratios, such as the Tropospheric Monitoring Instrument (TROPOMI) (Veefkind et al., 2012) on ESA's Sentinel 5 Precursor satellite, NASA's Earth Venture geostationary Tropospheric Emissions: Monitoring Pollution (TEMPO) (Zoogman et al., 2017), and NASA's Orbiting Carbon Observatory-3 (OCO-3) on the International Space Station (Eldering et al., 2019), will reduce the uncertainties in our top-down emissions method and provide estimates at higher temporal (daily) resolution.

Supplementary data to this article can be found online at https://doi.org/10.1016/j.scitotenv.2019.133805.

Acknowledgments

This publication was developed using funding from the NASA Atmospheric Composition Modeling and Analysis Program (ACMAP), program #: NNH16ZDA001N. This publication was also partially funded by the Department of Energy, Office of Fossil Energy, Office of Strategic Planning and Global Engagement. This publication was also developed under Assistance Agreement No. RD835871 awarded by the U.S. Environmental Protection Agency to Yale University. It has not been formally reviewed by EPA. The views expressed in this document are solely those of the SEARCH Center and do not necessarily reflect those of the Agency. EPA does not endorse any products or commercial services mentioned in this publication. OMI NO_2 data can be freely downloaded from the NASA website (doi: https://doi.org/10.5067/Aura/OMI/DATA2017). NO_X bottom-up emissions data can be found here: https://www.epa.gov/air-emissions-inventories/air-pollutant-emissions-trends-data. CO_2 bottom-up emissions data can be found here: https://www.epa.gov/statelocalenergy/state-co2-emissions-fossil-fuel-combustion. Annual continuous emission monitoring system (CEMS) data from power plants can be downloaded here: https://ampd.epa.gov/ampd/. The submitted manuscript has been created by UChicago Argonne, LLC, Operator of Argonne National Laboratory ("Argonne"). Argonne, a US Department of Energy Office of Science laboratory, is operated under contract no. DE-AC02-06CH11357.

References

Akingunola, A., Makar, P.A., Zhang, J., Darlington, A., Li, S.-M., Gordon, M., et al., 2018. A chemical transport model study of plume-rise and particle size distribution for the Athabasca oil sands. Atmos. Chem. Phys. 18 (12), 8667–8688. https://doi.org/10.5194/acp-18-8667-2018.

Beirle, S., Boersma, K.F., Platt, U., Lawrence, M.G., Wagner, T., 2011. Megacity emissions and lifetimes of nitrogen oxides probed from space. Science 333 (6050), 1737–1739. https://doi.org/10.1126/science.1207824.

Berezin, E.V., Konovalov, I.B., Ciais, P., Richter, A., Tao, S., Janssens-Maenhout, G., et al., 2013. Atmospheric chemistry and physics multiannual changes of CO_2 emissions in China: indirect estimates derived from satellite measurements of tropospheric NO_2 columns. Atmos. Chem. Phys. 13, 9415–9438. https://doi.org/10.5194/acp-13-9415-2013.

Crisp, D., Atlas, R., Breon, F.-M., Brown, L., Burrows, J., Ciais, P., et al., 2004. The Orbiting Carbon Observatory (OCO) mission. Adv. Space Res. 34 (4), 700–709. https://doi.org/10.1016/j.asr.2003.08.062.

Cui, X., Newman, S., Xu, X., Andrews, A.E., Miller, J., Lehman, S., et al., 2019. Atmospheric observation-based estimation of fossil fuel CO_2 emissions from regions of central and southern California. Sci. Total Environ. 664, 381–391. https://doi.org/10.1016/j.scitotenv.2019.01.081.

Dee, D.P., Uppala, S.M., Simmons, A.J., Berrisford, P., Poli, P., Kobayashi, S., et al., 2011. The ERA-Interim reanalysis: configuration and performance of the data assimilation system. Q. J. R. Meteorol. Soc. 137 (656), 553–597. https://doi.org/10.1002/qj.828.

Dobber, M., Kleipool, Q., Dirksen, R., Levelt, P.F., Jaross, G., Taylor, S., et al., 2008. Validation of ozone monitoring instrument level 1b data products. J. Geophys. Res. https://doi.org/10.1029/2007JD008665.

Eldering, A., Wennberg, P.O., Crisp, D., Schimel, D.S., Gunson, M.R., Chatterjee, A., et al., 2017. The Orbiting Carbon Observatory-2 early science investigations of regional carbon dioxide fluxes. Science https://doi.org/10.1126/science.aam5745.

Eldering, Annmarie, Taylor, T.E., Dell, C.W., Pavlick, R., 2019. The OCO-3 mission: measurement objectives and expected performance based on 1 year of simulated data. Atmospheric Measurement Techniques 12 (4), 2341–2370. https://doi.org/10.5194/amt-12-2341-2019.

de Foy, B., Wilkins, J.L., Lu, Z., Streets, D.G., Duncan, B.N., 2014. Model evaluation of methods for estimating surface emissions and chemical lifetimes from satellite data. Atmos. Environ. 98, 66–77. https://doi.org/10.1016/j.atmosenv.2014.08.051.

de Foy, B., Lu, Z., Streets, D.G., 2016. Impacts of control strategies, the Great Recession and weekday variations on NO_2 columns above North American cities. Atmos. Environ. 138 (2), 74–86. https://doi.org/10.1016/j.atmosenv.2016.04.038.

Gately, C.K., Hutyra, L.R., 2017. Large uncertainties in urban-scale carbon emissions. Journal of Geophysical Research: Atmospheres 122 (20), 11,242–11,260. https://doi.org/10.1002/2017JD027359.

Gately, Conor K., Hutyra, L.R., Sue Wing, I., 2015. Cities, traffic, and CO_2: a multidecadal assessment of trends, drivers, and scaling relationships. Proc. Natl. Acad. Sci. 112 (16), 4999–5004. https://doi.org/10.1073/pnas.1421723112.

Goldberg, D.L., Lamsal, L.N., Loughner, C.P., Swartz, W.H., Lu, Z., Streets, D.G., 2017. A high-resolution and observationally constrained OMI NO_2 satellite retrieval. Atmos. Chem. Phys. 17 (18), 11403–11421. https://doi.org/10.5194/acp-17-11403-2017.

Goldberg, D.L., Saide, P.E., Lamsal, L.N., de Foy, B., Lu, Z., Woo, J.-H., et al., 2019. A top-down assessment using OMI NO_2 suggests an underestimate in the NO_x emissions inventory in Seoul, South Korea, during KORUS-AQ. Atmos. Chem. Phys. 19 (3), 1801–1818. https://doi.org/10.5194/acp-19-1801-2019.

de Gouw, J.A., Parrish, D.D., Frost, G.J., Trainer, M., 2014. Reduced emissions of CO_2, NO_x, and SO_2 from U.S. power plants owing to switch from coal to natural gas with combined cycle technology. Earth's Future 2 (2), 75–82. https://doi.org/10.1002/2013EF000196.

Guo, M., Li, J., Xu, J., Wang, X., He, H., Wu, L., 2017. CO_2 emissions from the 2010 Russian wildfires using GOSAT data. Environ. Pollut. 226, 60–68. https://doi.org/10.1016/j.envpol.2017.04.014.

Gurney, K.R., Razlivanov, I., Song, Y., Zhou, Y., Benes, B., Abdul-Massih, M., 2012. Quantification of fossil fuel CO_2 emissions on the building/street scale for a large U.S. City. Environmental Science & Technology 46 (21), 12194–12202. https://doi.org/10.1021/es3011282.

Gurney, K.R., Liang, J., O'Keeffe, D., Patarasuk, R., Hutchins, M., Huang, J., et al., 2019. Comparison of global downscaled versus bottom-up fossil fuel CO_2 emissions at the urban scale in four US urban areas. Journal of Geophysical Research: Atmospheres https://doi.org/10.1029/2018JD028859.

Hakkarainen, J., Ialongo, I., Tamminen, J., 2016. Direct space-based observations of anthropogenic CO_2 emission areas from OCO-2. Geophys. Res. Lett. 43 (21), 11,400–11,406. https://doi.org/10.1002/2016GL070885.

Hammerling, D.M., Michalak, A.M., O'Dell, C., Kawa, S.R., 2012. Global CO_2 distributions over land from the Greenhouse Gases Observing Satellite (GOSAT). Geophys. Res. Lett. https://doi.org/10.1029/2012GL051203.

Hansen, J., Johnson, D., Lacis, A., Lebedeff, S., Lee, P., Rind, D., Russell, G., 1981. Climate impact of increasing atmospheric carbon dioxide. Science 213 (4511), 957–966. https://doi.org/10.1126/science.213.4511.957.

Hedelius, J.K., Liu, J., Oda, T., Maksyutov, S., Roehl, C.M., Iraci, L.T., et al., 2018. Southern California megacity CO_2, CH_4, and CO flux estimates using ground-and space-based remote sensing and a Lagrangian model. Atmos. Chem. Phys. 18, 16271–16291. https://doi.org/10.5194/acp-18-16271-2018.

International Energy Agency, 2008. World energy outlook. Retrieved from. https://www.iea.org/media/weowebsite/2008-1994/WEO2008.pdf.

IPCC, 2013. Climate change 2013 - the physical science basis. In: Intergovernmental Panel on Climate Change (Ed.), Climate Change 2013 the Physical Science Basis: Working Group I Contribution to the Fifth Assessment Report of the Intergovernmental Panel on Climate Change. Cambridge University Press, Cambridge https://doi.org/10.1017/CBO9781107415324.

Jiang, Z., McDonald, B.C., Worden, H., Worden, J.R., Miyazaki, K., Qu, Z., et al., 2018. Unexpected slowdown of US pollutant emission reduction in the past decade. Proc. Natl. Acad. Sci. 115 (20), 5099–5104. https://doi.org/10.1073/pnas.1801191115.

Konovalov, I.B., Berezin, E.V., Ciais, P., Broquet, G., Beekmann, M., Hadji-Lazaro, J., et al., 2014. Constraining CO_2 emissions from open biomass burning by satellite observations of co-emitted species: a method and its application to wildfires in Siberia. Atmos. Chem. Phys. 14, 10383–10410. https://doi.org/10.5194/acp-14-10383-2014.

Konovalov, I.B., Berezin, E.V., Ciais, P., Broquet, G., Zhuravlev, R.V., Janssens-Maenhout, G., 2016. Estimation of fossil-fuel CO_2 emissions using satellite measurements of "proxy" species. Atmos. Chem. Phys. 16 (21), 13509–13540. https://doi.org/10.5194/acp-16-13509-2016.

Kort, E.A., Frankenberg, C., Miller, C.E., Oda, T., 2012. Space-based observations of megacity carbon dioxide. Geophys. Res. Lett. 39 (17), 1–5. https://doi.org/10.1029/2012GL052738.

Krotkov, N.A., Lamsal, L.N., Celarier, E.A., Swartz, W.H., Marchenko, S.V., Bucsela, E.J., et al., 2017. The version 3 OMI NO_2 standard product. Atmospheric Measurement Techniques 10 (9), 3133–3149. https://doi.org/10.5194/amt-10-3133-2017.

Kuze, A., Suto, H., Nakajima, M., Hamazaki, T., 2009. Thermal and near infrared sensor for carbon observation Fourier-transform spectrometer on the Greenhouse Gases Observing Satellite for greenhouse gases monitoring. Appl. Opt. 48 (35), 6716. https://doi.org/10.1364/AO.48.006716.

Laughner, J.L., Zhu, Q., Cohen, R.C., 2019. Evaluation of version 3.0B of the BEHR OMI NO2 product. Atmospheric Measurement Techniques 12 (1), 129–146. https://doi.org/10.5194/amt-12-129-2019.

Lauvaux, T., Miles, N.L., Deng, A., Richardson, S.J., Cambaliza, M.O., Davis, K.J., et al., 2016. High-resolution atmospheric inversion of urban CO_2 emissions during the dormant season of the Indianapolis Flux Experiment (INFLUX). Journal of Geophysical Research: Atmospheres 121 (10), 5213–5236. https://doi.org/10.1002/2015JD024473.

Levelt, P.F., Oord, G.H.J. Van Den, Dobber, M.R., Dirksen, R.J., MÄLKKI, A., VISSER, H., et al., 2006. The ozone monitoring instrument. IEEE Trans. Geosci. Remote Sens. 44 (5), 1093–1101 (doi:Urn:nbn:nl:ui:25-648485).

Levelt, P.F., Joiner, J., Tamminen, J., Veefkind, J.P., Bhartia, P.K., Zweers, D.C.S., et al., 2018. The ozone monitoring instrument: overview of 14 years in space. Atmos. Chem. Phys. 18 (8), 5699–5745. https://doi.org/10.5194/acp-18-5699-2018.

Lu, Z., Streets, D.G., de Foy, B., Lamsal, L.N., Duncan, B.N., Xing, J., 2015. Emissions of nitrogen oxides from US urban areas: estimation from ozone monitoring instrument retrievals for 2005–2014. Atmos. Chem. Phys. 15 (18), 10367–10383. https://doi.org/10.5194/acp-15-10367-2015.

McLinden, C.A., Fioletov, V.E., Boersma, K.F., Kharol, S.K., Krotkov, N., Lamsal, L., et al., 2014. Improved satellite retrievals of NO_2 and SO_2 over the Canadian oil sands and comparisons with surface measurements. Atmos. Chem. Phys. 14 (7), 3637–3656. https://doi.org/10.5194/acp-14-3637-2014.

Mitchell, L.E., Lin, J.C., Bowling, D.R., Pataki, D.E., Strong, C., Schauer, A.J., et al., 2018. Long-term urban carbon dioxide observations reveal spatial and temporal dynamics related to urban characteristics and growth. Proc. Natl. Acad. Sci. 115 (12), 2912–2917. https://doi.org/10.1073/pnas.1702393115.

Nangini, C., Peregon, A., Ciais, P., Weddige, U., Vogel, F., Wang, J., et al., 2019. A global dataset of CO_2 emissions and ancillary data related to emissions for 343 cities. Scientific Data 6, 180280. https://doi.org/10.1038/sdata.2018.280.

Nassar, R., Hill, T.G., McLinden, C.A., Wunch, D., Jones, D.B.A., Crisp, D., 2017. Quantifying CO_2 emissions from individual power plants from space. Geophys. Res. Lett. 44 (19), 10,045–10,053. https://doi.org/10.1002/2017GL074702.

Oda, T., Maksyutov, S., 2011. A very high-resolution (1 km × 1 km) global fossil fuel CO_2 emission inventory derived using a point source database and satellite observations of nighttime lights. Atmos. Chem. Phys. https://doi.org/10.5194/acp-11-543-2011.

Oda, T., Maksyutov, S., Andres, R.J., 2018. The open-source data inventory for anthropogenic CO_2, version 2016 (ODIAC2016): a global monthly fossil fuel CO_2 gridded emissions data product for tracer transport simulations and surface flux inversions. Earth System Science Data https://doi.org/10.5194/essd-10-87-2018.

Patarasuk, R., Gurney, K.R., O'Keeffe, D., Song, Y., Huang, J., Rao, P., et al., 2016. Urban high-resolution fossil fuel CO_2 emissions quantification and exploration of emission drivers for potential policy applications. Urban Ecosyst. 19 (3), 1013–1039. https://doi.org/10.1007/s11252-016-0553-1.

Reuter, M., Buchwitz, M., Schneising, O., Krautwurst, S., O'Dell, C.W., Richter, A., et al., 2019. Towards monitoring localized CO_2 emissions from space: co-located regional CO_2 and NO_2 enhancements observed by the OCO-2 and S5P satellit. Atmospheric Chemistry and Physics Discussions, 1–19 https://doi.org/10.5194/acp-2019-15.

Russell, A.R., Valin, L.C., Cohen, R.C., 2012. Trends in OMI NO_2 observations over the United States: effects of emission control technology and the economic recession. Atmos. Chem. Phys. 12 (24), 12197–12209. https://doi.org/10.5194/acp-12-12197-2012.

Sargent, M., Barrera, Y., Nehrkorn, T., Hutyra, L.R., Gately, C.K., Jones, T., et al., 2018. Anthropogenic and biogenic CO_2 fluxes in the Boston urban region. Proc. Natl. Acad. Sci. 115 (29), 7491–7496. https://doi.org/10.1073/pnas.1803715115.

Schwandner, F.M., Gunson, M.R., Miller, C.E., Carn, S.A., Eldering, A., Krings, T., et al., 2017. Spaceborne detection of localized carbon dioxide sources. Science 358 (6360). https://doi.org/10.1126/science.aam5782.

Silvern, R.F., Jacob, D.J., Mickley, L.J., Sulprizio, M.P., Travis, K.R., Marais, E.A., et al., 2019. Using satellite observations of tropospheric NO_2 columns to infer long-term trends in US NO_x emissions: the importance of accounting for the free tropospheric NO_2 background. Atmos. Chem. Phys. 19 (13), 8863–8878. https://doi.org/10.5194/acp-19-8863-2019.

Tong, D.Q., Pan, L., Chen, W., Lamsal, L., Lee, P., Tang, Y., et al., 2016. Impact of the 2008 Global Recession on air quality over the United States: implications for surface ozone levels from changes in NO_x emissions. Geophys. Res. Lett. 43 (17), 9280–9288. https://doi.org/10.1002/2016GL069885.

Turnbull, J., Karion, A., Davis, K.J., Lauvaux, T., Miles, N.L., Richardson, S.J., et al., 2018. Synthesis of urban CO_2 emission estimates from multiple methods from the Indianapolis Flux Project (INFLUX). Environmental Science & Technology 53. https://doi.org/10.1021/acs.est.8b05552 acs.est.8b05552. research-article.

Valin, L.C., Russell, A.R., Hudman, R.C., Cohen, R.C., 2011. Effects of model resolution on the interpretation of satellite NO_2 observations. Atmos. Chem. Phys. 11 (22), 11647–11655. https://doi.org/10.5194/acp-11-11647-2011.

Valin, L.C., Russell, A.R., Cohen, R.C., 2013. Variations of OH radical in an urban plume inferred from NO_2 column measurements. Geophys. Res. Lett. 40 (9), 1856–1860. https://doi.org/10.1002/grl.50267.

Veefkind, J.P., Aben, I., McMullan, K., Förster, H., de Vries, J., Otter, G., et al., 2012. TROPOMI on the ESA Sentinel-5 Precursor: a GMES mission for global observations of the atmospheric composition for climate, air quality and ozone layer applications. Remote Sens. Environ. 120 (2012), 70–83. https://doi.org/10.1016/j.rse.2011.09.027.

Ye, X., Lauvaux, T., Kort, E.A., Oda, T., Feng, S., Lin, J.C., et al., 2017. Constraining fossil fuel CO_2 emissions from urban area using OCO-2 observations of total column CO_2. Atmospheric Chemistry and Physics Discussions, 1–30 https://doi.org/10.5194/acp-2017-1022.

Zoogman, P., Liu, X., Suleiman, R.M., Pennington, W.F., Flittner, D.E., Al-Saadi, J.A., et al., 2017. Tropospheric emissions: monitoring of pollution (TEMPO). J. Quant. Spectrosc. Radiat. Transf. 186 (2017), 17–39. https://doi.org/10.1016/j.jqsrt.2016.05.008.